# Measurements of inelastic energy loss and $K$-vacancy production in atomic collisions at keV energies and large scattering angles

B. Fastrup, G. Hermann, Q. Kessel,*† and A. Crone
*Institute of Physics, University of Aarhus, DK-8000 Aarhus C, Denmark*
(Received 4 March 1974)

The differential inelastic energy loss $Q$ has been determined for keV atomic collisions between $Na^+$, $Ne^+$, $Ne^{++}$, $F^+$, $O^+$, and $N^+$ projectiles and Ne, $N_2$, and $NH_3$ targets for scattering angles between 2° and 15°. The data, which have been obtained under single-collision conditions, determine the probability of producing a $K$ vacancy and the corresponding $K$-excitation energy for specified charge states of the projectile before and after the collision. The production of a $K$ vacancy has been shown to take place preferentially in the low-$Z$ collision partner with a probability depending on the collision's distance of closest approach and the projectile velocity. The data suggest that rotational coupling between the $2p\sigma$ molecular orbital (MO) and the $2p\pi$ MO produces the $K$ vacancy. The $K$-excitation probability is shown to depend strongly on the outer-shell ($2p$), precollisional configuration of the high-$Z$ collision partner. For $N^+$-$NH_3$, $Ne^+$-Ne, $Ne^{++}$-Ne, and $Na^+$-Ne collisions, the maximum $K$-excitation probabilities are 35%, (10–15)%, 20%, and $< 1$%, respectively. These observations are in accord with the Fano-Lichten model. For $N^+$ and $O^+$ projectiles incident on $N_2$ and $NH_3$ targets, triple-peaked $Q$ spectra occur, indicating a fair probability of the production of two $K$ vacancies. For asymmetric collision systems such as $O^+$-$NH_3$, the two $K$ vacancies are produced preferentially in the low-$Z$ collision partner.

## I. INTRODUCTION

The pioneering experimental investigations of $L$-shell excitations in violent $Ar^+$-Ar collisions, carried out in Connecticut by Everhart and coworkers[1] and in Leningrad by Fedorenko and coworkers,[2] revealed unexpectedly large cross sections for the production of $L$-shell vacancies. The subsequent explanation of these cross sections in terms of a molecular orbital (MO) model by Fano and Lichten[3] encouraged other laboratories to investigate the conditions under which inner-shell excitations are likely to occur in heavy ion-atom collisions. For reviews of the experiments up to 1972, the reader is referred to Kessel,[4] Kessel and Fastrup,[5] and Garcia, Fortner, and Kavanagh.[6] It is characteristic of these collisions that near-adiabatic conditions prevail during the collision and that single-electron molecular states (MO's) of the diabatic kind[7,8] form a suitable basis for the description of the excitation mechanism. Although the first experiments of Everhart and coworker and Fedorenko and co-workers dealt with inner-shell excitations in the symmetric collision systems $Ar^+$-Ar and $Ne^+$-Ne, it was later shown experimentally that asymmetric collisions of the type $Z_1^+$-Ar[9] exhibit characteristic features similar to those observed for Ar -Ar. An example of this is the occurrence of a triple-peaked inelastic energy-loss spectrum for certain distances of closest approach $R_0$. Although inelastic energy-loss data provide detailed information about the collision process—for example, determination of the differential cross section for the production of an inner-shell vacancy as a function of the collision energy, the scattering angle, and the final charge state of the scattered ions—only few laboratories have so far been involved in these time-consuming measurements.[5] A greater volume of inner-shell excitation data has been obtained by measuring the total emission yield versus energy of either Auger electrons[10] or characteristic x rays.[5,6] The cross sections obtained by the latter methods represent an integration over all impact parameters and charge states of the scattered particles. This inherent averaging makes it difficult to get detailed information of the collision process, e.g., its specific dependence on the collision velocity and on $R_0$, the collision's distance of closest approach. In the differential experiments reported here, where this information is obtained, it is possible to determine the characteristics of the various excitation mechanisms, for example, the location of significant crossings between MO's.

The Fano-Lichten model indicates that the MO excitations of $L$ and $M$ shells are caused primarily by potential couplings at a series of crossings.[5] Highly promoted diabatic $4f\sigma$ and $6h\sigma$ MO's appear to be responsible for the production of $L_{2,3}$ and $M_{4,5}$ vacancies, respectively. Within certain narrow ranges of $R_0$, each of these MO's cross other closely spaced MO's, and this multi-crossing-type of interaction leads to an inner-shell-excitation probability which is approximately unity if $R_0 < R_x$ and zero if $R_0 > R_x$, where $R_x$ represents the inter-

nuclear distance of the multi-crossing zone. In contrast to $L$- and $M$-shell excitations, which are intractable to theoretical computations, $K$-shell excitations represent a simpler and therefore particularly interesting situation from a theoretical point of view. The $K$ excitations are primarily due to a rotational coupling between two adjacent MO's, the $2p\sigma$ and the $2p\pi$ MO's, which are degenerate in the united-atom limit. This special feature of $K$ excitations makes them well suited for a detailed test of the validity of the MO model. It was originally predicted by Lichten[7] and subsequently verified by the Connecticut group[11] that for the symmetric Ne-Ne systems, such as in $Ne^0$, $Ne^+$, $Ne^{++}$-Ne collisions, the probability of producing a $K$ vacancy should depend on the charge state of the incident Ne particles. The reason for this is that at least one $2p\pi$ vacancy is needed to allow the transfer of a $K$ electron from the $2p\sigma$ MO to the $2p\pi$ MO during the collision. Since the $2p\pi$ MO in the separated-atom limit relates to the neon $2p$ orbital, this is the reason why the probability of producing a $K$ vacancy in neon depends on the number of neon $2p$ vacancies prior to the collision. This also explains why collision systems with at least a neon configuration exhibit a very low $K$-excitation cross section. This charge-state effect is frequently called the "exit-channel effect," i.e., the exit channel for a $K$ excitation is closed if no $2p\pi$ vacancies exist and is open when one or two $2p\pi$ vacancies exist. Because the rotational coupling can only couple the $2p\sigma$ MO with the $x$ component of the $2p\pi$ MO (i.e., the component in the scattering plane), at most two relevant $2p\pi_x$ vacancies can exist in the $2p\pi$ MO. The rotationally induced coupling between $2p\sigma$ and $2p\pi$ MO's was first discussed by Bates and Williams,[12] who showed the general characteristics of this type of coupling and its dependence on the collision velocity and the impact parameter.

The present paper describes a systematic and detailed experimental study of the $K$-excitation mechanism in heavy ion-atom collisions. Owing to the simple features of $K$ excitations, such measurements are particularly useful for testing the validity of the MO model. Symmetric and asymmetric collision systems with atomic numbers ranging from 7 to 11 have been studied by measuring the inelastic energy-loss spectra for various incident energies and scattering angles of the projectiles.

In selecting the collision systems, special emphasis has been placed on the study of the rotational coupling mechanism and of the exit-channel effect. $Na^+$, $Ne^+$, $Ne^{++}$, $F^+$, $O^+$, and $N^+$ projectiles are scattered by Ne, $N_2$, and $NH_3$ targets under single-collision conditions. The preliminary data presented earlier[13] showed general agreement with the Barat-Lichten MO model for asymmetric collisions.[14] The complete set of data presented here substantiates these earlier findings. Recently Briggs and Macek[15] have performed a two-state, perturbed stationary-state calculation of the $K$-excitation cross section in $Ne^+$-Ne and $N^+$-N collisions. Their calculations, which include electron-translational factors, agree well with our Ne-Ne data, whereas there is some disagreement between their calculated data for the N-N system and our experimental data for the N-$N_2$ system.

## II. EXPERIMENTAL METHOD

The apparatus and the experimental method have been described in detail earlier,[9] and only a brief review will be given here. For the lower incident ion energies, the isotopically pure beams are supplied by an 80-keV isotope separator, and for the higher ion energies, a 500-keV accelerator is used. Both these accelerators are equipped with universal ion sources of the Nielsen type.[16] When an entrance collimating system has reduced the beam divergence to $\frac{1}{3}°$, incident ions with an energy $E_0$ enter a differentially pumped scattering chamber containing the target gas. The scattering chamber is divided into two parts: a fixed lower part into which the incident ions enter, and a rotatable upper part with a collimating system which selects the particles which have been scattered through an angle $\theta$. After this collimation, the ions pass through a cylindrical electrostatic analyzer and into an open electron multiplier, which detects the energy-analyzed particles. This system is capable of determining the energy $E_1$ and the charge state $m$ of the particles scattered through a given angle $\theta$, which can be varied from zero to 132°.

Single-collision conditions are ensured by keeping the product of the target-gas pressure and the path length of the ions in the target below $10^{-3}$ Torr cm. Under these conditions, the number of scattered particles in each charge state $m$ is a linear function of the gas pressure. While the same criterion is applied when molecular gas targets are used, it may be questioned whether true single collisions are possible for these cases. To illustrate this point further, consider the $N^+$-$N_2$ collision system. Since the bond length of an $N_2$ molecule is approximately 1 Å, while the collisions being investigated have values of $R_0$ which are less than 0.15 Å, geometrical considerations show that the likelihood of the incident nitrogen ion coming within a distance of 0.15 Å of both the nitrogen atoms in the $N_2$ molecule is negligible. From this point of view it is possible to study

single collisions using molecular targets.

From the measured values of $E_0$, $E_1$, and $\theta$, the inelastic energy loss $Q$ can be found through conservation of energy and momentum. The resulting formula for $Q$ is

$$Q = 2\gamma(E_1E_0)^{1/2}\cos\theta - (1+\gamma)E_1 + (1-\gamma)E_0, \quad (1)$$

where $\gamma$ is the projectile-to-target-mass ratio $M_1/M_2$. This method of determining $Q$, called the scattered-particle method, has been shown to produce spectra whose widths are not seriously affected by thermal motion of the target atoms.[9] This being true, the experimentally observed linewidths in the energy spectra have two primary contributions: a natural linewidth and an instrumental width. Although the natural linewidth is appreciable[17] and comparable with the observed width, in the present data there also exists a contribution from fluctuations in the beam energy. However, for the purpose of determining the separate and distinct energy losses and the corresponding number of events in each line, this indeterminancy of the natural linewidth is of no practical consequence. As shown in Eq. (1), the calculated $Q$ values depend on $\gamma$ and therefore on the isotopic weight of the target atoms (the beam being isotopically pure). In the case of neon target atoms, commercial pure neon gas is used. The isotopic abundances in neon are: 90.92% of $^{20}$Ne, 8.82% of $^{22}$Ne, and 0.25% of $^{21}$Ne. When compared to the $^{20}$Ne $Q$ spectra (see, e.g., Fig. 1), the data are easily corrected for this effect. Our experimental method did not allow a determination of the energy spectrum of the neutrals in the scattered beam. For most of the collisions investigated here, the charge-state distribution of the scattered ions is such that the number of neutral atoms in the scattered beam is estimated to be less than 5% and of minor importance in the present investigation.

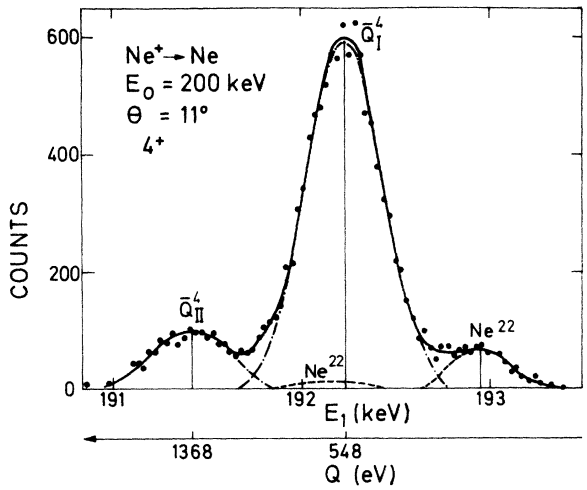


FIG. 1. Energy spectrum of the scattered 4+ neon ions from $Ne^+$-Ne collisions with incident energy $E_0$ = 200 keV and scattering angle $\theta = 11°$. The contributions from $^{22}$Ne target atoms are indicated.

Except for the presence of a $^{22}$Ne peak when neon targets are used, the majority of the inelastic energy-loss spectra have single or double values. In a double-valued $Q$ spectrum, the lower $Q$ line will here be denoted by $\bar{Q}_{\rm I}$ and the higher $Q$ line by $\bar{Q}_{\rm II}$. Figure 1 shows an example of a double-peaked $Q$ spectrum for the case of $Ne^+$-Ne collisions. From such spectra, the $Q$ values $\bar{Q}_j^m$ and the excitation probabilities $P_j^m$ corresponding to charge state $m$ of the scattered incident particles and peak $j$ (= I, II) are obtained. From these basic data, we derive $\bar{Q}_j$, the mean $Q$ for peak $j$ weighted over the charge-state distribution and the excitation probability $P_j$ of exciting $Q_j$. Also derived is $\bar{m}_j$, the mean-charge state of the scattered incident particles from the $Q_j$ excited collisions. The precise definitions of these quantities are given in Ref. 9. Owing to long-term fluctuations in the beam energy, the absolute values of the peak positions in the $Q$ spectra, ($\bar{Q}_{\rm I}$ and $\bar{Q}_{\rm II}$) may be somewhat unprecise (in rare cases up to 20%), but the quantity of interest in connection with inner-shell excitations, $\bar{Q}_{\rm II} - \bar{Q}_{\rm I}$, is good to better than 5%. The uncertainties on $P_{\rm II}$ and $\bar{m}_j$ are estimated to be ±0.015 and ±0.15 charge units, respectively.

## III. DATA AND RESULTS

### A. Atomic-target case: $Na^+$, $Ne^+$, $Ne^{++}$, $F^+$, $O^+$, and $N^+$-Ne

$Na^+$-Ne: The data are obtained at 200 keV and at scattering angles from 7° to 20°. The $R_0$ values[18] for these collisions range from 0.06 to 0.03 Å. Under these conditions, the $Q$ spectrum is single-valued, an example of which is shown in Fig. 2, where only a $Q_{\rm I}$ type of excitation is observed.

Although the $Q$ data show no sign of a second peak which would correspond to a $K$ excitation, we cannot completely rule out the possibility of a very small $K$-excitation probability. In Fig. 2 we see that $\bar{Q}_{\rm I} = 664$ eV, and by simply adding the $K$-binding energy of neon (870 eV) we obtain an estimate of the position of a possible $\bar{Q}_{\rm II}$ peak to be 664 + 870 = 1534 eV. At this position, Fig. 2 shows a completely flat energy distribution with a height less than 1% of the peak value in the observed $Q_{\rm I}$ distribution. Hence we may argue that the probability of producing a $K$ vacancy in $Na^+$ → Ne collisions is less than 1%. In this respect it is worthwhile to note that both the incident $Na^+$

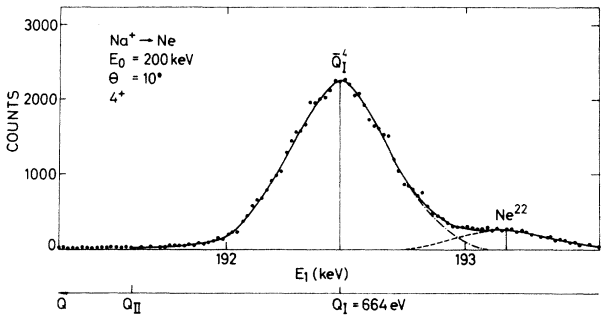


FIG. 2. Energy spectrum of the scattered 4+ sodium ions from $Na^+$-Ne collisions with incident energy $E_0$ = 200 keV and scattering angle $\theta = 10°$. The estimated position of a possible $Q_{II}$ peak is indicated.

ion and the Ne target atom have complete $2p$ subshells and therefore, according to the MO model, should not permit the formation of any $2p\pi$ vacancies. The $Na^+$-Ne collision system is an example of a system with a so-called closed-exit channel for $K$ excitation. The mean-charge state $\bar{m}_I$, which is displayed against $E_0\theta$ in Fig. 3, is approximately 3 and is nearly independent of the scattering angle $\theta$, i.e., of $R_0$.

$KLL$ Auger-emission cross sections,[19] measured as a function of incident ion energy, agree well with these exit-channel arguments.[5,7] The electron data show that for $Na^{++}$-Ne collisions, where the high-$Z$ partner has one $2p$ vacancy before the collision, the probability of producing a $K$ vacancy at low energies (<100 keV) is one or two orders of magnitude higher than for $Na^+$-Ne collisions where no $2p$ vacancies exist before the collision. It is further observed that the emission cross sections for $Ne^+$-Ne and $Na^{++}$-Ne collisions are nearly identical at the same velocities.

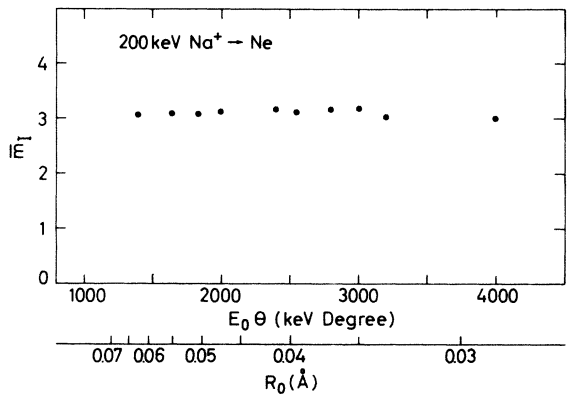


FIG. 3. Mean charge state $\bar{m}_I$ of the scattered sodium ions from 200 keV $Na^+$-Ne collisions as a function of the product $E_0\theta$ and the corresponding distance of closest approach $R_0$.

$Ne^+$, $Ne^{++}$-Ne: The data are obtained at 150, 200, 300, and 400 keV for $Ne^+$-Ne and at 300 keV for $Ne^{++}$-Ne collisions. The scattering angles range from 3° to 15° and the corresponding $R_0$ values from 0.09 to 0.022 Å. In most cases, the measured energy spectra are double-valued, indicating two different modes of excitation, $Q_I$ and $Q_{II}$. Figure 4 shows $\bar{Q}_j$ and $\bar{m}_j$ as a function of $E_0\theta$. The difference $\bar{Q}_{II}$-$\bar{Q}_I$ is nearly constant and equal to 860 eV. This value corresponds well with the binding energy of a neon-$K$ electron, 870 eV. This suggests that a $Q_{II}$ excitation involves the excitation of a single neon-$K$ electron, whereas a $Q_I$ excitation involves only excitations among the outer ($n=2$) electrons. The difference $\bar{m}_{II}$-$\bar{m}_I$ is constant and equal to 0.45, which, under the assumption that half the $K$ excitations take place in the projectile ions, infers that a $K$ excitation changes the sum of the mean-charge states of both

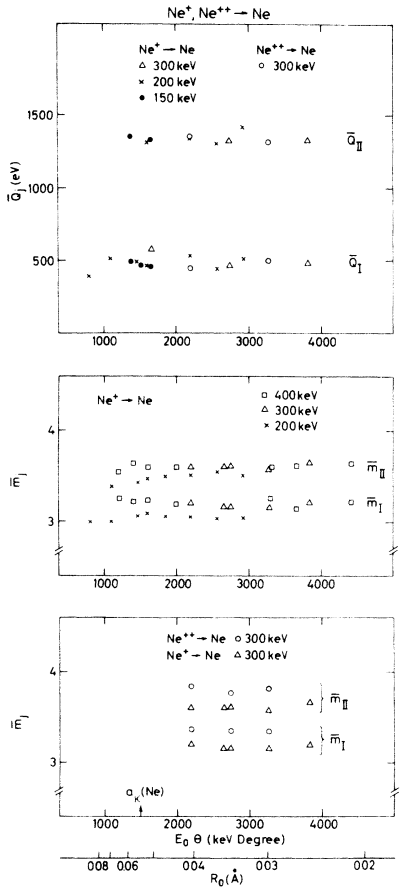


FIG. 4. $Ne^+$-Ne and $Ne^{++}$-Ne: mean inelastic energy loss $\bar{Q}_j$ and mean charge state $\bar{m}_j$ of the scattered neon particles as a function of the product $E_0\theta$ and $R_0$. A comparison of $\bar{m}_j$ values obtained from 300 keV $Ne^+$-Ne and 300 keV $Ne^{++}$-Ne collisions is given. The $K$-shell radius for a neon atom $a_K$(Ne) is indicated.

atoms by 0.9. This change may be partly accounted for by the *KLL* Auger process following a *K* excitation, whereby a *K* electron is promoted into a $2p\pi$ vacancy, leaving a $2p\sigma$ vacancy which subsequently decays by an Auger process. In Fig. 5 is shown the probability $P_{II}$ of producing a single *K* vacancy in either neon-collision partner. There is an appreciable dependence of $P_{II}$ on the primary energy $E_0$ for fixed values of the product $E_0\theta$ or equivalently $R_0$. Further, a strong dependence of $P_{II}$ on the initial charge state of the incident particles is noted, i.e., $Ne^{++}$-Ne collisions are almost twice as efficient in producing *K* vacancies as are $Ne^{+}$-Ne collisions when both cases are measured under otherwise identical conditions. This charge-state effect was originally estimated by Lichten[7] to be two, and shortly afterwards this value was confirmed experimentally[11] by the determination of the *KLL* Auger-emission yields for incident 200 keV $Ne^{+}$ and $Ne^{++}$ ions on neon atoms. Our more detailed *Q* studies at 300 keV, however, show that the charge-state effect is definitely less than two and approximately equal to 1.7. This value is in good accordance with recent *KLL*-emission data[19] obtained over an extended energy range from 80 to 500 keV. At low energies, the charge-state effect is found to be approximately two, but the value decreases slowly with increasing energy.

$F^{+}$-Ne: The data are obtained at 200 keV and at scattering angles ranging from 6° to 9°. The $\bar{Q}_j$, $P_j$, and $\bar{m}_j$ data are shown in Fig. 6. The difference $\bar{Q}_{II}$-$\bar{Q}_I$ is 680 eV, which corresponds well with the fluorine *K*-binding energy of 686 eV.

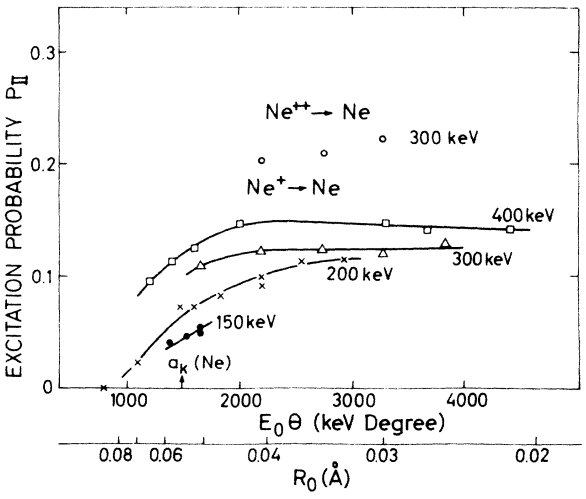


FIG. 5. $Ne^{+}$-Ne and $Ne^{++}$-Ne: probability for producing one *K*-shell vacancy $P_{II}$ as a function of the product $E_0\theta$ and $R_0$. The *K*-shell radius for a neon atom $a_K$(Ne) is indicated.

This suggests that *K* excitations take place predominantly in fluorine. This conclusion is further supported by the charge-state data of the scattered fluorine ions, where it is found that $\bar{m}_{II}$-$\bar{m}_I$ is approximately unity.

$O^{+}$-Ne: Only a few energy spectra are obtained for $O^{+}$-Ne collisions. An example is shown in Fig. 7, which clearly demonstrates the existence of a double-peaked structure. The energy separation of these peaks indicates that the *K* vacancy is produced primarily in the oxygen ion. On the basis of similar data, obtained by a delayed-coincidence technique, Bingham and Rice[20] arrived at the same conclusion.

$N^{+}$-Ne: The data are obtained at 60, 125, 160, and 200 keV and at scattering angles ranging from 2° to 15°. In these collisions, the small energy separation (400 eV) between the two *Q* peaks, $\bar{Q}_I$ and $\bar{Q}_{II}$, together with the small *K*-excitation probability $P_{II}$, makes it difficult to quantitatively resolve the energy spectra. Hence, some of the results shown are not as accurate as those obtained in other collision systems, where either the $P_{II}$ values or the $\bar{Q}_{II}$-$\bar{Q}_I$ differences are substantially higher than for the $N^{+}$-Ne collisions.

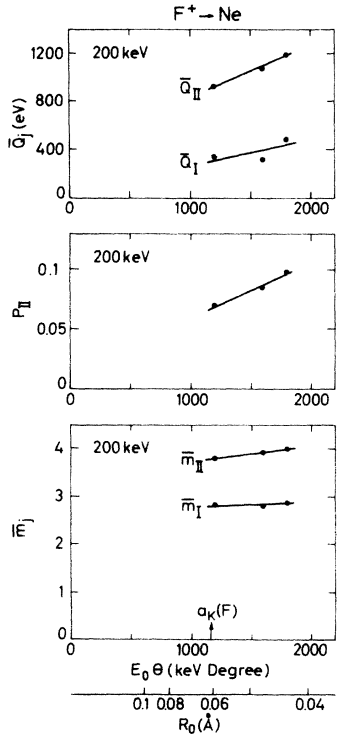


FIG. 6. $F^{+}$-Ne: mean inelastic energy loss $\bar{Q}_j$, probability for producing one *K*-shell vacancy in fluorine $P_{II}$, and mean charge state $\bar{m}_j$ of the scattered fluorine particles as a function of the product $E_0\theta$ and $R_0$. The *K*-shell radius for a fluorine atom $a_K(F)$ is indicated.

The $P_{II}$ results are shown in Fig. 8. Although the points show some scatter around the fitted lines, it is apparent that $P_{II}$ depends upon both $E_0\theta$ and $E_0$. In Fig. 8, the mean-charge state $\bar{m}_I$ is plotted as a function of $E_0\theta$. It is curious to note that for $E_0\theta$ exceeding approximately 250 keV× degrees, $\bar{m}_I$ is fairly constant and equal to 2.2 over the measured range of $E_0\theta$ values. Owing to difficulties with the resolution of the measured energy spectra, we have not been able to obtain reliable $\bar{Q}_I$ and $\bar{Q}_{II}$ results. The data are, however, consistent with the $K$ vacancy being formed preferentially in the low-$Z$ partner, i.e., the nitrogen ion.

### B. Molecular-target case: $Na^+$, $Ne^+$, $O^+$, and $N^+$-$N_2$, $NH_3$

For the collisions under consideration here, inner-shell excitations are produced by close encounters, the trajectories of which may be treated classically. As noted in the section dealing with experimental method, it is highly unlikely for a projectile to suffer such a close encounter with more than one of the atoms comprising the molecular target.

In spite of this, the presence of a molecular partner in the target can cause a substantial perturbation of the inner-shell excitation probability $P_{II}$. Measurements by Fastrup and Crone[21] on systems such as $C^+$, $N^+$, and $O^+$ incident on molecular targets of $N_2$ and $NH_3$, and $N^+$ on $O_2$ and $H_2O$ targets, clearly demonstrate this effect. Their $N^+$-$NH_3$ and $N^+$-$N_2$ data show that the probability of a $K$ excitation is about 12% higher for the $N^+$-$N_2$ collisions than it is for the $N^+$-$NH_3$ collisions. A similar effect was not observed for $Ne^+$-$N_2$ and $Ne^+$-$NH_3$ collisons. The data of Fastrup and Crone may be summarized as follows: In homonuclear collisions, such as $N^+$-$N_2$ and $N^+$-$NH_3$ and collisions for which the projectile is the low-$Z$ collision partner, the probability $P_{II}$ does depend on the molecular nature of the target. However, if the molecule contains the lighter collision partner, then there seems to be no molecular effect.

The explanation of these molecular effects is uncertain. From collisions with atomic targets it is clear that the promotion probability depends primarily on two factors: First, a rotational coupling when the $2p\sigma$ and $2p\pi$ MO's are nearly degenerate, and second, a $2p\pi$ vacancy into which the promoted electron may go. Of these two factors it would seem that the second of these, the exit-channel factor, is the one most likely to be affected by the neighboring atoms in a molecular target. For the case of a low-$Z$ projectile incident on a high-$Z$ target atom, $P_{II}$ depends on the number of $2p$ vacancies carried into the $2p\pi$ MO by the target atom. When this target atom is part of a molecule, it is likely, as Fastrup and Crone note, that the presence of a molecular neighbor somehow increases the probability of a vacancy appearing in the $2p\pi$ MO during the collision.

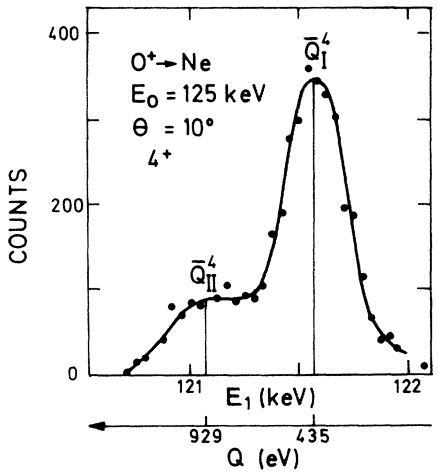


FIG. 7. Energy spectrum of the scattered 4+ oxygen ions from $O^+$-Ne collisions with incident energy $E_0$ = 125 keV and scattering angle $\theta = 10°$.

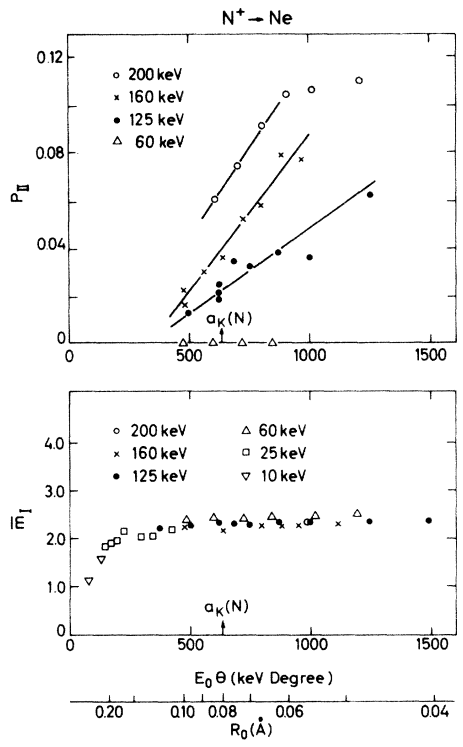


FIG. 8. $N^+$-Ne: probability for producing one $K$-shell vacancy in nitrogen $P_{II}$, and mean charge state $\bar{m}_I$ of the scattered nitrogen particles as a function of the product $E_0\theta$ and $R_0$. The $K$-shell radius for a nitrogen atom $a_K$(N) is indicated.

$Na^+$-$N_2$: The data are obtained at 200 keV and at a 6° scattering angle. The energy spectra for charge-states 1–4 of the scattered sodium ions are recorded, and in all cases only a single-peaked spectrum is observed. $\bar{Q}_I$ is found to be 424 eV and $\bar{m}_I$ to be 2.6. A spectrum for $m=2$ is shown in Fig. 9. To put an upper boundary on the probability of producing a $K$ excitation in nitrogen, we may argue as follows: A possible $\bar{Q}_{II}$ line should be positioned at approximately $424+400=824$ eV. This value falls within the tail of the $Q_I$ distribution such that from the experimental data, $P_{II}$ can be estimated to be less than 5%.

$Ne^+$-$N_2$, $NH_3$: The data are obtained at 180 keV, which is the same relative velocity as for the 125-keV $N^+$-Ne collisions discussed earlier. The scattering angles range from 3° to 6°. The $\bar{Q}_j$, $P_j$, and $\bar{m}_j$ curves are shown in Fig. 10. $\bar{Q}_{II}$-$\bar{Q}_I$ is a constant difference of 370 eV, which is in good agreement with the binding energy (400 eV) of a nitrogen $K$ electron. The $P_{II}$ curve or the $K$-excitation probability is seen to be independent of the target being $N_2$ or $NH_3$. Within the experimental uncertainty, $\bar{m}_I=\bar{m}_{II}\simeq 2.5$. This shows that a $K$ excitation in the collision system does not alter the resulting mean-charge state of the scattered incident particle (the neon ion). The $Q$- and charge-state data are consistent with the hypothesis[13,14] that the $K$ excitation take place preferentially in the low-$Z$ collision partner, i.e., the nitrogen particle.

$O^+$-$N_2$, $NH_3$: The data are obtained at 183 keV and at scattering angles ranging from 2.5° to 3.5°. These data normally show a double-peaked $Q$ structure, but in a few cases a third peak ($Q_{III}$) is found, as shown in Fig. 11. The observation of a triple-peaked $Q$ structure in the case of $O^+$-$NH_3$ suggests that the largest $Q$ value ($Q_{III}$) corresponds to the production of two $K$ vacancies in the nitrogen-target particle. This assumption is supported by the fact that the difference $\bar{Q}_{III}$-$\bar{Q}_{II}$ is only slightly higher than $\bar{Q}_{II}$-$\bar{Q}_I$, the latter value (400 eV) agreeing well with the binding energy of a single $K$ electron in nitrogen (the binding energy of a single $K$ electron in oxygen is 535 eV and definitely higher than the measured $\bar{Q}_{III}$-$\bar{Q}_{II}$ value). The $\bar{Q}_j$, $P_j$, and $\bar{m}_j$ curves are shown in Fig. 12. The difference $\bar{Q}_{II}$-$\bar{Q}_I$ is seen to be independent

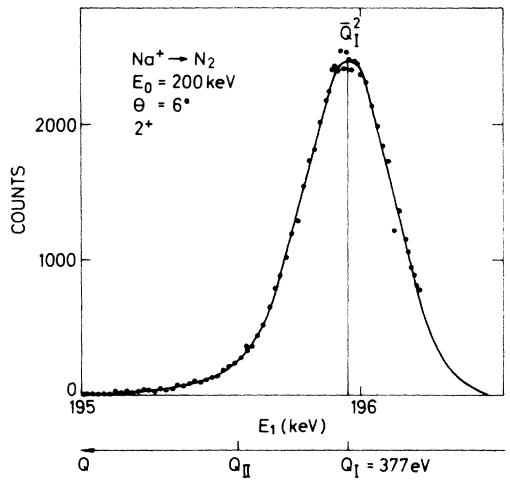


FIG. 9. Energy spectrum of the scattered 2+ sodium ions from $Na^+$-$N_2$ collisions with incident energy $E_0$ = 200 keV and scattering angle $\theta=6°$. The estimated position of a possible $Q_{II}$ peak is indicated.

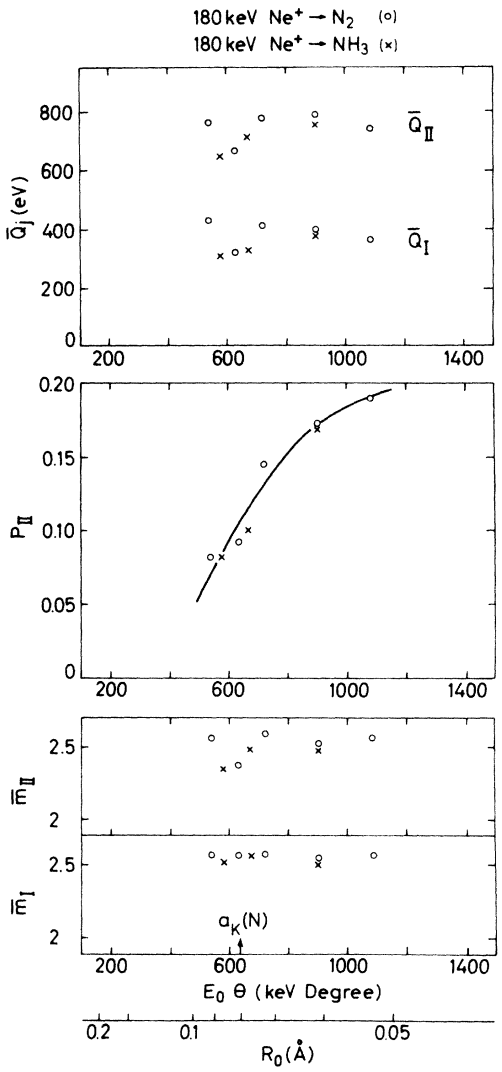


FIG. 10. $Ne^+$-$N_2$ and $Ne^+$-$NH_3$: mean inelastic energy loss $\bar{Q}_j$, probability for producing one $K$-shell vacancy in nitrogen $P_{II}$, and the mean charge state $\bar{m}_j$ of the scattered neon particles as a function of the product $E_0\theta$ and $R_0$. The $K$-shell radius for a nitrogen atom, $a_K$(N), is indicated.

of $E_0\theta$. The probability of a $K$ excitation, $P_{II}$, seems not to depend upon the nature of the molecular target containing the nitrogen atom(s). We note that $P_{II}$ for $O^+$-$N_2$, $NH_3$ collisions is appreciably higher than for $Ne^+$-$N_2$, $NH_3$ collisions. The lower curves in Fig. 12 show that the mean-charge states $\bar{m}_I$ and $\bar{m}_{II}$ are approximately equal. This is consistent with the general finding that the $K$ excitation is being produced in the low-$Z$ collision partner, i.e., in the nitrogen particle.

$N^+$-$N_2$, $NH_3$: In the case of $N^+$-$N_2$ collisions, a more detailed study of the conditions under which $K$ vacancies are produced is carried out. Primary energies of 50, 70, 125, and 160 keV are used, and the particles being scattered have been energy-analyzed for several scattering angles in the range from 3° to 14°. Almost all energy spectra reveal a double-peaked structure, but a few cases at high values of the product $E_0\theta$ show also a third peak ($Q_{III}$). The data are shown in Figs. 13(a)–13(f), where $\bar{Q}_j$, $P_j$, and $\bar{m}_j$ are plotted versus $E_0\theta$. The $\bar{Q}_j$ data plotted in Figs. 13(a) and 13(b) show that although $\bar{Q}_I$ and $\bar{Q}_{II}$ depend slightly upon the primary energy $E_0$, their difference $\bar{Q}_{II} - \bar{Q}_I$ is found to be fairly constant and equal to 400 eV, the binding energy of a single $K$ electron in nitrogen. The data plotted in Fig. 13(c) show that the probability of producing a single $K$ vacancy, $P_{II}$, depends not only on $E_0\theta$ (or $R_0$) but also upon the primary energy. The $P_{II}$'s appear to have a threshold such that no $K$ excitations occur if $E_0\theta$ is smaller than 200 keV×degree or, alternatively, if $R_0$ is larger than 0.15 Å. This latter value is somewhat smaller than twice the $K$ radius in nitrogen. Figure 13(d) shows the $P_{II}$'s for 160-keV $N^+$-$N_2$ and $N^+$-$NH_3$ collisions. The slight but definite difference between the two curves is presumably due to a molecular effect.[21] The $\bar{m}_j$ curves in Fig. 13(f) for 160-keV incident $N^+$ ions on $N_2$ and $NH_3$ targets show that the mean-charge states $\bar{m}_I$ and $\bar{m}_{II}$ are independent of the scattering angle $\theta$, $E_0\theta$, and of the nature of the molecule. The latter feature supports the earlier assumption that violent ion-molecule encounters are essentially binary ion-atom encounters. The difference $\bar{m}_{II} - \bar{m}_I$ is 0.45; this is consistent with half of the $K$ excitations occurring in the projectile ions.

For $N^+$-$NH_3$ collisions, where only one nitrogen atom is present in the molecular target, the data are obtained at 160 keV and at scattering angles from 2.4° to 5°. These data show a triple-peaked structure in the energy spectra, an example of which is shown in Fig. 14. From such data, anal-

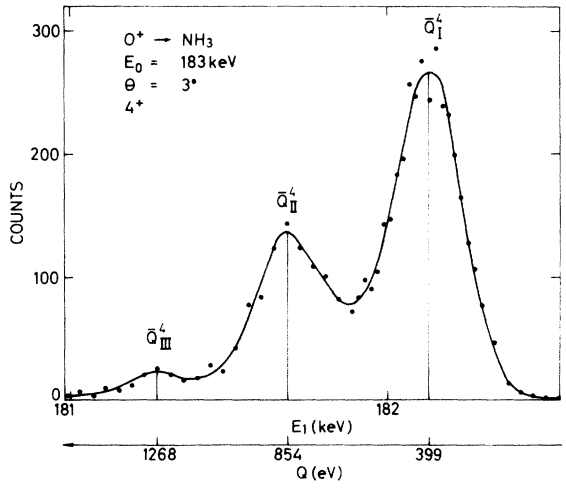


FIG. 11. Energy spectrum of the scattered 4+ oxygen ions from $O^+$-$NH_3$ collisions with incident energy $E_0$ = 183 keV and scattering angle $\theta = 3°$.

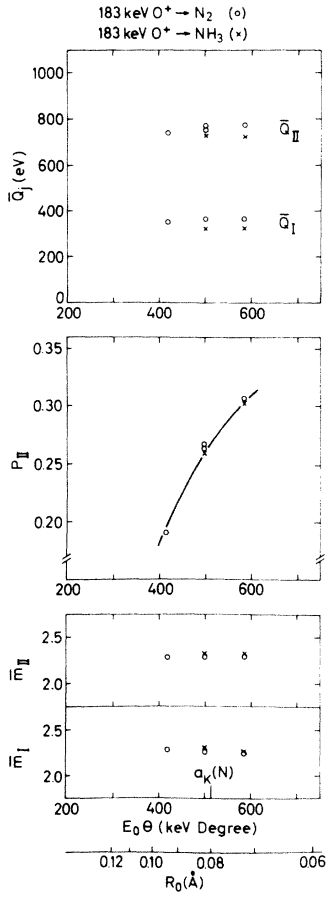


FIG. 12. $O^+$-$N_2$ and $O^+$-$NH_3$: mean inelastic energy loss $\bar{Q}_j$, probability for producing one $K$-shell vacancy in nitrogen, $P_{II}$, and mean charge state $\bar{m}_j$ of the scattered oxygen particles as a function of the product $E_0\theta$ and $R_0$. The $K$-shell radius for a nitrogen atom $a_K$(N) is indicated.

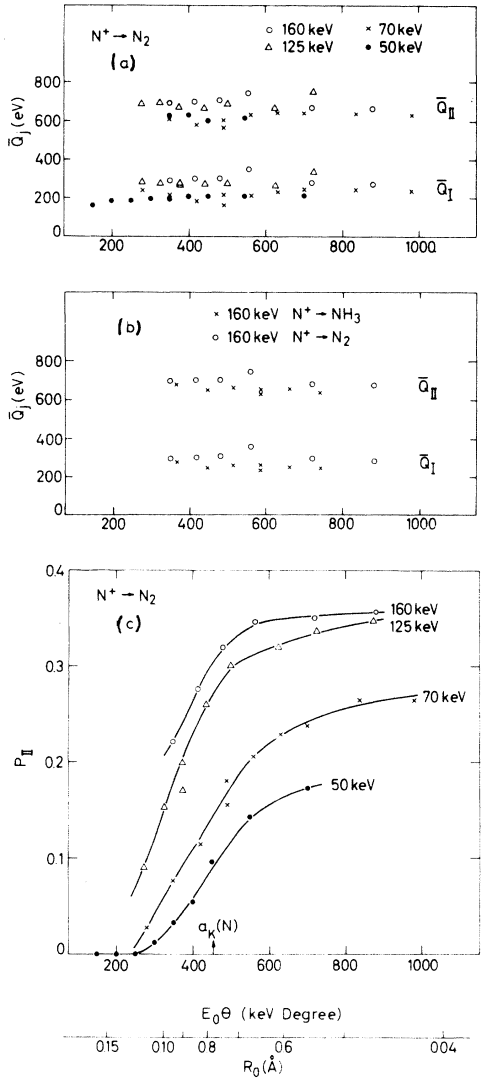


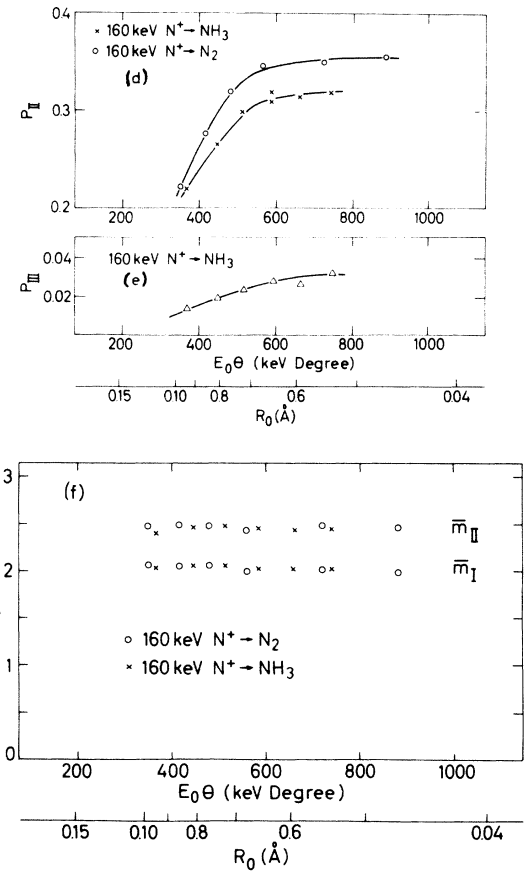


FIG. 13. $N^+$-$N_2$ and $N^+$-$NH_3$: (a)–(b) mean inelastic energy loss $\bar{Q}_j$, (c)–(d) probability for producing one $K$-shell vacancy $P_{II}$, (e) probability for producing two $K$-vacancies, $P_{III}$, and (f) mean charge state $\bar{m}_j$ of the scattered nitrogen particles. The data are plotted vs the product $E_0\theta$ and $R_0$. The $K$-shell radius for a nitrogen atom $a_K(N)$ is indicated

ysis has yielded $P_{III}$, the probability of producing two $K$ vacancies, as a function of $E_0\theta$ [see Fig. 13(e)].

### C. Charge-state distributions

A selection of typical charge-state distributions $P_j(m)$ for different collision systems is shown in Fig. 15. These examples clearly demonstrate that the fraction of neutrals in the scattered, incident beam is very small and that inclusion of these neutrals in the previous data analysis will not alter the results significantly. The different plots illustrate how the charge-state distribution is affected by a $K$-excitation process. If the $K$ excitation takes place in the projectile, as in the $F^+$-Ne collisions of Fig. 15(a), its charge-state distributions for $Q_I$ and $Q_{II}$ excitations, $P_I(m)$ and $P_{II}(m)$, respectively, will have similar shapes, but the distribu-

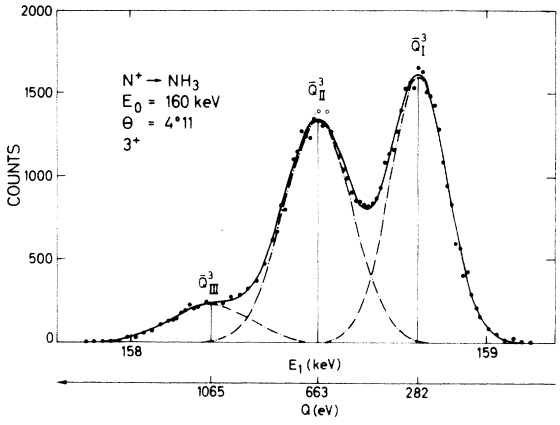


FIG. 14. Energy spectrum of the scattered 3+ nitrogen ions from $N^+$-$NH_3$ collisions with incident energy $E_0$ = 160 keV and scattering angle $\theta = 4.11°$. The dashed lines show the separated peaks.

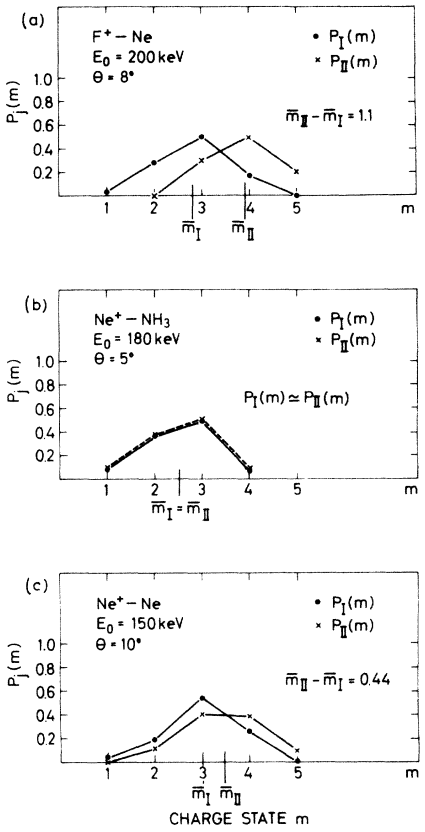


FIG. 15. Charge-state distributions $P_j(m)$ ($j$ = I,II) for different collision systems (a) $F^+$-Ne, (b) $Ne^+$-$NH_3$, and (c) $Ne^+$-Ne. The values of the mean charge states $\bar{m}_j$ are indicated.

tions are separated by a charge-state difference of approximately unity. When the $K$ excitation takes place in the target atom, as in the $Ne^+$-$NH_3$ collisions of Fig. 15(b), the charge-state distributions of the scattered, incident particles are unaffected by the $K$ excitation. For symmetric collisions such as $Ne^+$-Ne [Fig. 15(c)] and $N^+$-$N_2$, half of the $K$ excitations occur in the projectile ions and half in the target particles. For this situation, the measured charge-state distributions $P_I(m)$ and $P_{II}(m)$ of the scattered, incident particles are separated by approximately 0.45. This value is in reasonable agreement with the expectation that an inner-shell excitation in one of the collision partners will shift the charge-state distribution of that atom by approximately unity.

## IV. DISCUSSION

The data, presented in a condensed form in Tables I and II, show several general features which are listed below.

(i) In cases where the high-$Z$ collision partner initially has one or more $2p$ vacancies, there is an appreciable probability (between 10% and 40%) of a $K$ excitation for sufficiently low $R_0$ values and sufficiently high relative nuclear velocities. The probability increases with the number of initial $2p$ vacancies in the high-$Z$ partner.

(ii) If the high-$Z$ collision partner has initially a filled $2p$ subshell, we must distinguish between two cases, i.e., one where the low-$Z$ partner is initially neutral, and one where it is initially

TABLE I. Atomic target case. Presentation of $\bar{Q}_I, \bar{m}_I$, the differences $\bar{Q}_{II}-\bar{Q}_I$ and $\bar{m}_{II}-\bar{m}_I$, and the maximum probability for producing one $K$-shell vacancy $P_{II}^{max}$ for the various collision cases studied. $\bar{Q}_{II}-\bar{Q}_I$ is compared with the binding energy of a $K$ electron in the projectile atom $E_K(Z_1)$. When possible, the critical distance of closest approach $R_c$ for producing a $K$-shell vacancy is given and compared with the sum of the $K$-shell radii of the colliding particles, $a_K(Z_1)+a_K(Z_2)$. The collisions are characterized by the energy $E_0$ and velocity $v_0$ of the incident ion and by the product $E_0\theta$ and correspondingly the distance of closest approach $R_0$ (see Ref. 18).

| $Z_1^{i+}$-$Z_2$ | $E_0$ (keV) | $v_0$ ($10^8$ cm/sec) | $E_0\theta$ (keV× degrees) | $R_0$ (Å) | $R_c$ (Å) | $a_K(Z_1)+a_K(Z_2)$ (Å) | $\bar{Q}_I$ (eV) | $\bar{Q}_{II}-\bar{Q}_I$ (eV) | $\bar{m}_I$ | $\bar{m}_{II}-\bar{m}_I$ | $P_{II}^{max}$ | $E_K(Z_1)$ (eV) |
|---|---|---|---|---|---|---|---|---|---|---|---|---|
| $Na^+$-Ne | 200 | 1.30 | 1400–4000 | 0.063–0.032 | | 0.105 | 690 | | 3.1 | | $0^{+0.01}_{-0}$ | 1075 |
| $Ne^+$-Ne | 150 | 1.20 | 1350–1650 | 0.059–0.050 | | 0.110 | 500 | 860 | 3.0 | 0.45 | >0.05 | 870 |
| | 200 | 1.39 | 800–2900 | 0.088–0.033 | 0.08 | | 500 | 860 | 3.05 | 0.45 | 0.12 | |
| | 300 | 1.70 | 1650–3800 | 0.049–0.025 | | | 500 | 860 | 3.2 | 0.45 | 0.13 | |
| | 400 | 1.97 | 1150–4400 | 0.065–0.021 | | | 500 | 860 | 3.2 | 0.45 | 0.15 | |
| $Ne^{++}$-Ne | 300 | 1.70 | 2200–3300 | 0.040–0.028 | | 0.110 | 500 | 860 | 3.35 | 0.45 | 0.22 | 870 |
| $F^+$-Ne | 200 | 1.43 | 1200–1800 | 0.059–0.043 | | 0.116 | 380 | 680 | 2.8 | 1.1 | >0.1 | 690 |
| $O^+$-Ne | 125 | 1.23 | 1250 | 0.053 | | 0.124 | 380 | 500 [a] | 2.5 | | | 535 |
| $N^+$-Ne | 60 | 0.91 | 480–850 | 0.102–0.068 | | 0.135 | | 400 [a] | 2.2 | | 0 | 400 |
| | 125 | 1.31 | 500–1260 | 0.097–0.047 | 0.125 | | | 400 [a] | 2.2 | | >0.06 | |
| | 160 | 1.49 | 480–970 | 0.099–0.057 | 0.125 | | | 400 [a] | 2.2 | | >0.08 | |
| | 200 | 1.66 | 600–1200 | 0.084–0.048 | | | | 400 [a] | 2.2 | | >0.11 | |

[a] The experimental uncertainty of these values is ±50 eV. In all other cases $\bar{Q}_{II}-\bar{Q}_I$ is good to better than 5%.

TABLE II. Molecular-target case. Presentation of $\bar{Q}_I, \bar{m}_I$, the differences $\bar{Q}_{II}-\bar{Q}_I$ and $\bar{m}_{II}-\bar{m}_I$, and the maximum probabilities $P_{II}^{max}$ and $P_{III}^{max}$ for producing one and two $K$-shell vacancies, respectively, for the various collision cases studied. When possible, the critical distance of closest approach $R_c$ for producing a $K$-shell vacancy is given and compared with the sum of the $K$-shell radii of the colliding particles, $a_K(Z_1)+a_K(Z_2)$. The collisions are characterized by the energy $E_0$ and velocity $v_0$ of the incident ion and by the product $E_0\theta$ and correspondingly by the distance of closest approach $R_0$ (see Ref 18).

| $Z_1^{i+}$-$Z_2$ | $E_0$ (keV) | $v_0$ ($10^8$ cm/sec) | $E_0\theta$ (keV × degrees) | $R_0$ (Å) | $R_c$ (Å) | $a_K(Z_1)+a_K(Z_2)$ (Å) | $\bar{Q}_I$ (eV) | $\bar{Q}_{II}-\bar{Q}_I$ (eV) | $\bar{m}_I$ | $\bar{m}_{II}-\bar{m}_I$ | $P_{II}^{max}$ | $P_{III}^{max}$ |
|---|---|---|---|---|---|---|---|---|---|---|---|---|
| $Na^+$-$N_2$ | 200 | 1.30 | 1200 | 0.053 | | 0.130 | 425 | | 2.6 | | $0^{+0.03}_{-0}$ | |
| $Ne^+$-$N_2$ | 180 | 1.32 | 550–1100 | 0.090–0.053 | | 0.135 | 370 | 370 | 2.6 | 0 | >0.18 | |
| $Ne^+$-$NH_3$ | 180 | 1.32 | 580–910 | 0.087–0.061 | | 0.135 | 330 | 370 | 2.5 | 0 | >0.18 | |
| $O^+$-$N_2$ | 183 | 1.49 | 440–780 | 0.090–0.057 | | 0.150 | 360 | 400 | 2.3 | 0 | >0.3 | |
| $O^+$-$NH_3$ | 183 | 1.49 | 600–780 | 0.071–0.057 | | 0.150 | 320 | 400 | 2.3 | 0 | >0.3 | |
| $N^+$-$N_2$ | 50 | 0.83 | 140–700 | 0.183–0.061 | 0.13 | 0.160 | 200 | 400 | 1.7 | 0.42 | 0.19 | |
| | 70 | 0.98 | 240–980 | 0.130–0.046 | 0.14 | | 240 | 400 | 1.8 | 0.42 | 0.27 | |
| | 125 | 1.31 | 270–870 | 0.119–0.047 | 0.16 | | 280 | 400 | 2.1 | 0.42 | 0.35 | |
| | 160 | 1.49 | 340–870 | 0.100–0.047 | | | 300 | 400 | 2.1 | 0.42 | 0.36 | |
| $N^+$-$NH_3$ | 160 | 1.49 | 370–740 | 0.094–0.054 | | 0.160 | 245 | 400 | 2.1 | 0.42 | 0.32 | 0.03 |

charged. In the former case, as in $Na^+$-Ne, $N_2$ collisions, no $K$ excitations are observed. In the latter case, as in $N^+$-Ne collisions, a small but definite probability of a $K$ excitation is observed (see Fig. 16).

(iii) The probability of producing a $K$ vacancy depends not only on $R_0$, but also on $E_0$. When plotted versus $R_0$ or $E_0\theta$ (at constant $E_0$), the probability of producing a $K$ vacancy rises slowly from a threshold and reaches a maximum level which is generally small compared to unity and which depends on $E_0$. These features are all different from the way the $L_{2,3}$ and $M_{4,5}$ excitation probabilities behave. For example, these latter probabilities depend primarily on $R_0$ and show a very distinct threshold behavior, such that they rise steeply from an onset to a maximum value close to unity.

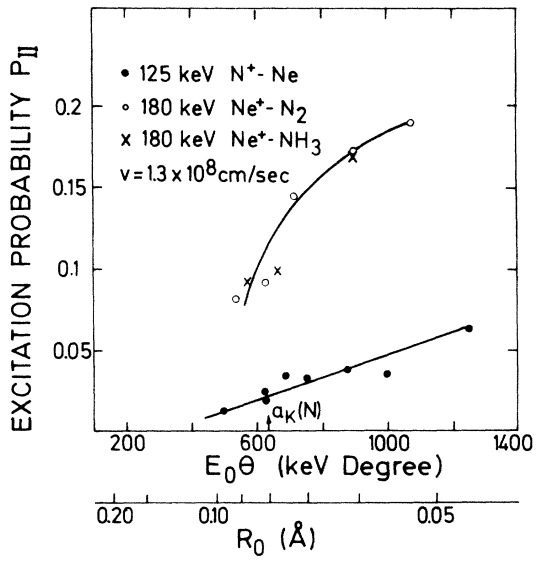


FIG. 16. $N^+$-Ne, $Ne^+$-$N_2$, and $Ne^+$-$NH_3$: probabilities for producing one $K$-shell vacancy in nitrogen $P_{II}$ at the same relative collision velocity $v=1.3\times10^8$ cm/sec as a function of the product $E_0\theta$ and $R_0$. The $K$-shell radius for a nitrogen atom $a_K$(N) is indicated.

(iv) If a collision results in a $K$ excitation, this is predominantly produced in the low-$Z$ collision partner or, in the case of symmetric collisions, in either partner with equal probability.

(v) The critical distance of closest approach $R_c$ for producing a $K$ vacancy is smaller than the sum of the $K$-shell radii of the two colliding particles, indicating that an appreciable overlap between the $K$-electron clouds of the two particles occurs during the collision.

(vi) For collisions of the types $O^+$-$N_2$, $NH_3$ and $N^+$-$N_2$, $NH_3$, triple-peaked $Q$ distributions are observed. The $Q_{III}$ peak corresponds to the production of two $K$ vacancies. In the case of $O^+$-$NH_3$, these two $K$ vacancies are both created in the nitrogen target atom, whereas in the case of $N^+$-$N_2$, $NH_3$, one $K$ vacancy is produced in each of the nitrogen particles, the projectile ion, and the target atom. As mentioned earlier, the chance of simultaneously producing a $K$ vacancy in both of the nitrogen target atoms in a $N_2$ molecule is negligible.

(vii) The charge-state distributions for a $Q_I$ and a $Q_{II}$ excitation are almost independent of $E_0\theta$ for the combinations of $E_0$ and $\theta$ investigated here.

(viii) A $K$ excitation affects the charge-state distribution of only that collision partner in which the $K$ excitation is produced. The net effect of a $K$ excitation and its subsequent decay is to raise

the charge state of that ion by approximately unity. Because of the small fluorescence yields of the atoms investigated here, the $K$ vacancies are expected to decay preferentially through Auger-electron emission.

Several of these observations may be understood within the framework of the MO model. Figures 17 and 18 show diabatic MO-correlation diagrams for symmetric and asymmetric collision systems. These diagrams, which show schematically the diabatic MO correlations between the orbitals of the united atom and the separated atoms, give a qualitative understanding of the mechanisms responsible for the production of inner-shell vacancies. With regard to the creation of a $K$ vacancy, a vacancy in the atomic $2p$ shell of one of the collision partners may become a vacancy in the $2p\pi$ MO of the molecule formed when the two nuclei approach each other during the collision. At small internuclear distances $R$, the $2p\pi$ MO and the $2p\sigma$ MO approach each other and become degenerate in the united-atom limit ($R=0$). Due to the fast rotation of the internuclear line $\vec{R}$ at small values of $R$, a significant coupling between the $2p\pi_x$ component (lying in the scattering plane) and the $2p\sigma$ MO takes place. Through this coupling, the $2p\pi$ vacancy may be transferred to the $2p\sigma$ MO. After the collision, when the nuclei separate, such a $2p\sigma$ vacancy becomes a hole in the $1s$ shell of one of the ions, i.e., a $K$ vacancy. For symmetric collisions, the $K$ vacancy is produced in either partner with the same probability. For asymmetric collisions, the $K$ vacancy is produced preferentially in the low-$Z$ partner, although the chance of producing it in the high-$Z$ partner becomes significantly higher when the atomic numbers of the partners differ only slightly.

For symmetric collision systems (see Fig. 17) the number of resulting $2p\pi$ vacancies is roughly proportional to the total number of atomic $2p$ vacancies present before the collision.[7] Since only $2p\pi_x$ vacancies can interact with the $2p\sigma$ MO, and since at most two $2p\pi_x$ vacancies exist, it is apparent that the statistical chance of transferring an atomic $2p$ vacancy to the $2p\pi_x$ state is approximately one sixth.[7,15] This explains why for $Ne^+ \rightarrow Ne$ collisions, $P_{II}$ is at most 15% and for $Ne^{++}$-Ne collisions at most 30%. If, instead, we consider $N^+$-N collisions (in our experiment $N^+$-$N_2$, $NH_3$), there exist seven (out of twelve possible) atomic $2p$ vacancies. For this reason, $P_{II}$ values in $N^+$-N collisions are substantially higher than for the $Ne^+$-Ne collisions. It is, however, a fact that we cannot apply the simple statistical estimates to obtain the resulting number of $2p\pi_x$ vacancies for the $N^+ \rightarrow N$ system. As pointed out by Macek and Briggs,[15] more elaborate methods have to be used in the case of more initial $2p$ vacancies. If the two colliding atoms have initially filled $2p$ subshells, as in $Ne^0$-Ne collisions, no

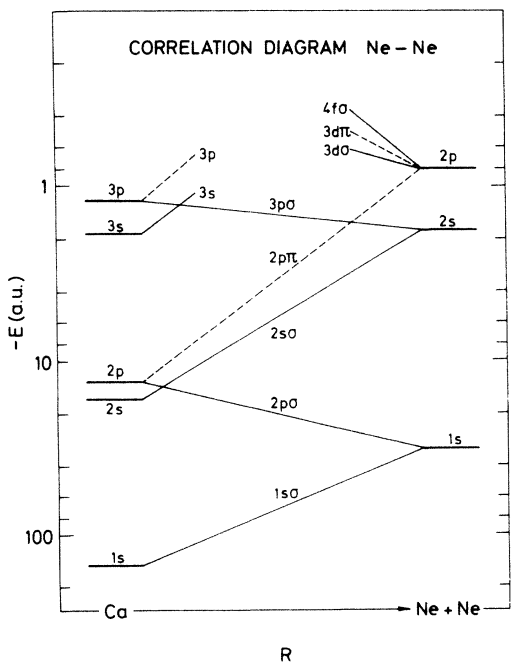


FIG. 17. Diabatic correlation diagram for the symmetric Ne-Ne system.

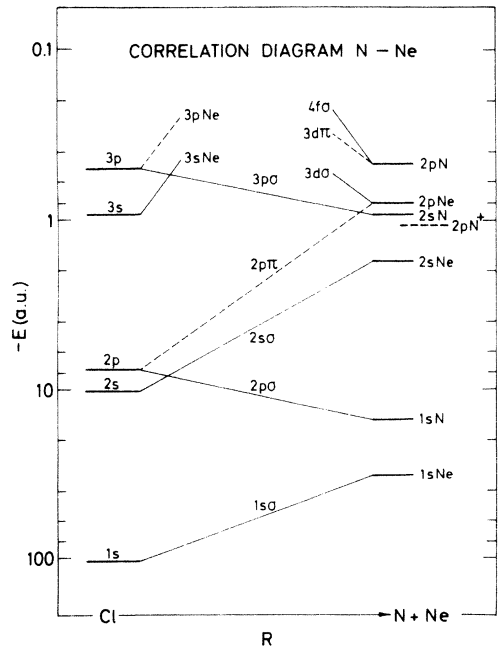


FIG. 18. Diabatic correlation diagram for the asymmetric N-Ne system. The ionization energy of $N^+$ is indicated.

$2p\pi_x$ vacancies will be created during the collision and, accordingly, the probability of producing a $K$ vacancy is expected to be extremely small. Experimental studies by McCaughey *et al.*[11] of the $KLL$ emission yield at 200 keV for $Ne^0$, $Ne^+$, and $Ne^{++}$-Ne gave the surprising result that the emission yield for $Ne^0$ - Ne collisions is 60% of that found for $Ne^+$ - Ne collisions. This has been a puzzle, and it has been suggested that the incident $Ne^0$ atoms might not be in the ground state. Very recent $KLL$ Auger-electron studies of $Na^+$, $Na^{++}$, $Ne^+$, and $Ne^{++}$-Ne[19] indicate that the emission yield for a closed $2p$-subshell configuration ($Na^+$-Ne) is indeed very low.

Next, consider the asymmetric collision systems represented by the correlation diagram in Fig. 18. Here the $2p$ orbitals of the colliding atoms are no longer degenerate. In this case, the $2p\pi$ MO correlates with a specific atomic $2p$ orbital when $R \to \infty$. This orbital is the $2p$ orbital of the high-$Z$ collision partner. The chance that an initial $2p$ vacancy in the high-$Z$ partner may become a $2p\pi_x$ vacancy is approximately one third.[15] If such a $2p\pi_x$ vacancy does exist, the rotational coupling between this state and the $2p\sigma$ MO may cause the transfer of that vacancy into the $2p\sigma$ MO. Then, as the nuclei separate after the collision, this vacancy becomes a $K$ vacancy in the low-$Z$ collision partner. Although our $Ne^+$-$N_2$ data do not extend to sufficiently high values of the product $E_0\theta$, the data clearly demonstrate that $P_{II}$ for $Ne^+$-N collisions is higher than for the symmetric $Ne^+$-Ne collisions. This effect is presumably due to the higher vacancy-occupation probability $N_\pi$ for the asymmetric $Ne^+$-N collisions ($N_\pi = \frac{1}{3}$), as compared to the symmetric $Ne^+$-Ne ($N_\pi = \frac{1}{6}$).

If the high-$Z$ collision partner has a closed $2p$ subshell, as in $Na^+$-Ne and $Na^+$-$N_2$, the collision system has a closed exit channel for a $K$ excitation. The experimental data for these collision systems revealed no $Q_{II}$ structure in agreement with this. The $KLL$ Auger-electron studies of the same collision systems[19] show that the emission cross sections are indeed very small and an order of magnitude smaller than if an initial $2p$ vacancy exists in the high-$Z$ partner, e.g., for $Na^{++}$-Ne and $Na^{++}$-$N_2$ collisions.

In some cases, the experimental results are not consistent with the simple estimates obtained from the schematic diabatic correlation diagrams. Let us illustrate this by an example: Figure 16 shows $P_{II}$ values plotted versus $E_0\theta$ for $Ne^+$-$N_2$ and $N^+$-Ne collisions, both measured at the same relative collision velocity. To a first approximation, we can disregard molecular effects ($N$ is the low-$Z$ collision partner and for $Ne^+$-$N_2$ and $Ne^+$-$NH_3$, the $P_{II}$'s are practically identical), and the experimental data show that $P_{II}$ for $Ne^+$-N collisions is approximately three times higher than for the reverse $N^+$-Ne collisions. According to the diabatic correlation diagram (see Fig. 18), the exit channel for a $K$ excitation is closed for the $N^+$-Ne system and open for the $Ne^+$-N system. This should result in an extremely small value of $P_{II}$ for the $N^+$-Ne collisions. As shown in Fig. 16, the experimental data do not support this prediction because this $P_{II}$, while smaller than for the $Ne^+$-N system, is certainly not zero. We may ask whether this is an example of a breakdown of the MO model; in a way, this does seem to be the case. However, because in the $N^+$-Ne system, the binding energy for the $2p$ electron in $N^+$ is higher than in Ne (see Fig. 18), the exit channel might not be completely closed. The probability of bringing an original nitrogen $2p$ vacancy down into the $2p\pi$ MO is apparently appreciable. It is possible that such a process of transferring a $2p$ vacancy from nitrogen into the $2p\pi$ MO may be due to dynamic coupling between near-degenerate MO's, perhaps the $3d\pi$ and $2p\pi$ MO's in this case. Such long-range, dynamic coupling, which could transfer vacancies into the $2p\pi$ MO, should be velocity-dependent. At low velocities, the coupling is small and the exit channel effectively closed. At higher velocities, the coupling can be substantial and the exit channel open. If we combine all the factors determining the $K$-excitation probability in one expression, we get

$$P_{II} = [N_\pi(o) + N_\pi(v)]P_{rot}, \tag{2}$$

where $N_\pi(o)$ is the static vacancy-occupation probability, as defined by Briggs and Macek,[15] $N_\pi(v)$ is a dynamic vacancy-occupation probability, which is zero at small velocities and increases with increasing velocity, and $P_{rot}$ determines the probability of transferring a vacancy from the $2p\pi_x$ state to the $2p\sigma$ MO. The essential features of the above expression are in good agreement with experimental data on $KLL$ Auger-emission yields[19] for the same systems as investigated here. This suggests that the simple, two-state $2p\pi$-$2p\sigma$ rotational-coupling approximation is reasonable if the exit channel for a $K$ excitation is open, i.e., there exists an initial $2p$ vacancy in the high-$Z$ collision partner. Thus, at not too high velocities, $N_\pi(o) \gg N_\pi(v)$, and Eq. (2) reduces to the well-known formula: $P_{II} = N_\pi(o)P_{rot}$. In the case of a closed exit channel, $N_\pi(o) = 0$ and Eq. (2) becomes: $P_{II} = N_\pi(v)P_{rot}$. Since the dynamic vacancy occupation probability $N_\pi(v)$ is governed by intermediate- or long-range coupling between the $2p\pi$ MO and other, unfilled, outer MO's and the $2p\pi$-$2p\sigma$ rotational coupling is most efficient at very small internuclear separation distances, we may still calculate $P_{rot}$ in a

two-state approximation. $N_\pi(v)$ is small, if either the collision velocity is small or the intermediate or long-range couplings are small. The latter situation occurs when the energy spacing between the $2p\pi$ MO and those other unfilled MO's is large, e.g., $Na^+$-Ne and $Na^+$-N. For such cases, the $K$ excitation probability is seen to be very small. If neither of these conditions are fulfilled, as in $N^+$-Ne, the $K$ excitation probability gets appreciable.

Briggs and Macek have written a series of papers dealing with the production of $K$-shell vacancies in symmetric ion-atom collisions.[15] Their model works within the framework of the one-electron approach of Fano and Lichten[3,7] and assumes $K$-shell promotion is due to an electronic transition from the $2p\sigma$ to the $2p\pi$ MO. Briggs and Macek first calculate the probability $N_\pi(o)$ of a $2p$ vacancy in the separated-atom limit becoming a vacancy in the $2p\pi$ MO and then calculate the probability $P_{\text{rot}}$ of a $2p\sigma$ electron filling it. For this latter step, they use a two-state perturbed stationary-state approximation which includes electron translational factors, i.e., takes account of the translational motion of the electron being excited. Since Briggs and Macek use a static calculation to estimate the probability that a $2p$ vacancy becomes a $2p\pi$ vacancy, their calculations may be somewhat unreliable in cases where the dynamic probability $N_\pi(v)$ is applicable, cf., the preceding discussion of Eq. (2). Their $P_{\text{II}}$ results for $Ne^+$-Ne at 200 keV are in satisfactory agreement with our experimental data, whereas their $P_{\text{II}}$ results for $N^+$-N at 160 keV deviate appreciably from our experimental $N^+$-$N_2$, $NH_3$ data. Even $N_\pi(o)$ may change a little from $N^+$-N to $N^+$-$N_2$ or $N^+$-$NH_3$; this is not sufficient to explain why the theoretical results are approximately 50% higher than the experimental results for $N^+$-N collisions.

## ACKNOWLEDGMENTS

The patient and effective assistance of members of the staff at the Institute of Physics is gratefully appreciated.

---

*Partial support received from the National Science Foundation.

†Permanent address: Department of Physics, University of Connecticut, Storrs, Conn. 06268.

[1]Q. C. Kessel and E. Everhart, Phys. Rev. 146, 16 (1966).

[2]V. V. Afrosimov, Yu. S. Gordeev, M. M. Panov, and N. V. Fedorenko, Zh. Tekh. Fiz. 34, 1613 (1964); 34, 1624 (1964); 34, 1637 (1964) [Sov. Phys.-Tech. Phys. 9, 1248 (1965); 9, 1256 (1965); 9, 1265 (1965)].

[3]U. Fano and W. Lichten, Phys. Rev. Lett. 14, 627 (1965).

[4]Q. C. Kessel, in *Case Studies in Atomic Collision Physics I*, edited by E. W. McDaniel and M. R. C. McDowell (North-Holland, Amsterdam, 1969), pp. 399–462.

[5]Q. C. Kessel and B. Fastrup, Case Studies in Atomic Phys. 3, 137 (1973).

[6]J. C. Garcia, R. J. Fortner, and T. M. Kavanagh, Rev. Mod. Phys. 45, 111 (1973).

[7]W. Lichten, Phys. Rev. 164, 131 (1967).

[8]F. T. Smith, Phys. Rev. 179, 111 (1969).

[9]B. Fastrup, G. Hermann, and K. J. Smith, Phys. Rev. A 3, 1591 (1971).

[10]M. E. Rudd and J. H. Macek, Case Studies in Atomic Phys. 3, 47 (1972).

[11]M. P. McCaughey, E. J. Knystautas, H. C. Hayden, and E. Everhart, Phys. Rev. Lett. 21, 65 (1968).

[12]D. R. Bates and D. A. Williams, Proc. Phys. Soc. 83, 425 (1964).

[13]B. Fastrup, G. Hermann, and Q. C. Kessel, Phys. Rev. Lett. 27, 771 (1971); 27, 1102 (1971).

[14]M. Barat and W. Lichten, Phys. Rev. A 6, 211 (1972).

[15]J. S. Briggs and J. H. Macek, J. Phys. B 6, 982 (1973); see also: J. S. Briggs and J. H. Macek, J. Phys. B 5, 579 (1972) and J. H. Macek and J. S. Briggs, J. Phys. B 6, 841 (1973).

[16]K. O. Nielsen, Nucl. Instrum. Methods 1, 289 (1957).

[17]V. V. Afrosimov, Yu. S. Gordeev, A. M. Polyanskii, and A. P. Shergin, Zh. Eksp. Theor. Fiz. 57, 806 (1969) [Sov. Phys.—JETP 30, 441 (1970)].

[18]The $R_0$ values in this paper have been calculated using a screened Coulomb potential following the method of M. T. Robinson, ORNL-3493; see also E. Everhart, G. Stone, and R. J. Carbone, Phys. Rev. 99, 1287 (1955).

[19]B. Fastrup, E. Bøving, G. A. Larsen, and P. Dahl, J. Phys. B (to be published); see also B. Fastrup and G. A. Larsen, in *Abstracts of the Seventh International Conference on the Physics of Electronic and Atomic Collisions*, edited by L. Branscomb *et al.* (North-Holland, Amsterdam, 1971), pp. 392–394.

[20]F. W. Bingham and J. K. Rice, Phys. Rev. A 6, 1819 (1972).

[21]B. Fastrup and A. Crone, Phys. Rev. Lett. 29, 825 (1972).